

Three-Vector Model Predictive Current Control of Permanent Magnet Assisted Synchronous Reluctance Motor Based on Step-by-Step Parameter Identification

Aide Xu^{2,*}, Ruijie Liu¹, and Yubang Yu¹

¹College of Electrical Engineering of Ships, Dalian Maritime University, Dalian 116026, China

²College of Information and Science Technology, Dalian Maritime University, Dalian 116026, China

ABSTRACT: This paper addresses the susceptibility of motor parameters to external disturbances during the operation of three-vector model predictive current control (TV-MPCC) for permanent magnet-assisted synchronous reluctance motors (PMA-SynRMs), which leads to increased current fluctuations and reduced tracking precision. To enhance the control system's stability, a step-by-step parameter identification approach is proposed. First, the proposed method devises six switching configurations, considers eight potential current prediction points generated by voltage vectors, and reformulates the value function. Next, a model reference adaptive system (MRAS) is employed to incrementally identify the motor's d and q axis inductances, resistance, and flux linkage. These identified parameters are used to update the model in real time. In this study, a 3 kW PMA-SynRM serves as the control object for simulation verification. Results indicate that the TV-MPCC based on step-by-step parameter identification has obvious improvement in current tracking static error and peak value of current fluctuation.

1. INTRODUCTION

In recent years, science and technology has been developed in the low-carbon, energy-efficient, and high-efficiency direction, and the research and application of clean energy are essential [1]. PMA-SynRM, as an efficient motor with a few rare earths, has a wide application prospect [2, 3]. It combines the benefits of permanent magnet synchronous motors and synchronous reluctance motors, typically utilizing ferrite pole materials, which has the characteristics of low cost, large saliency pole ratio, and straightforward control of demagnetization current [4–6]. PMA-SynRM torque mainly is derived from reluctance torque, which is usually controlled by Maximum Torque Per Ampere (MTPA) [7].

Model predictive control (MPC) can handle multi-objective control and has the advantage of fast dynamic response. Finite-set MPCC can directly act on the inverter with discrete switching states. However, only one switching state is applied per control cycle, which can lead to significant current fluctuations in the steady state. Refs. [8, 9] propose a two-vector MPCC strategy adding a second voltage vector to the single vector. This enables the synthesis of voltage vectors in arbitrary directions, effectively reducing current fluctuations. In [10, 11], a TV-MPCC strategy is introduced, adding a zero-voltage vector to the two-vector scheme which makes the resultant voltage vector close to the expected value.

During PMA-SynRM operation, motor parameters vary with changes in current, and the motor parameters may be mismatched due to disturbance, which will affect the TV-MPCC

performance. To address parameter mismatch, MRAS [12] is usually used to adjust the parameters of the prediction model online. In [13], an MPCC strategy with parameter identification function is introduced, which calculates the identification value of inductance parameters through model reference adaptive rate, and corrects the identification result to the control system in real time. Since PMA-SynRM contains only two voltage equations, identifying more than two parameters often leads to an under-rank problem in the identification equation. To overcome this issue, it is necessary to either reduce the number of identified parameters or increase the number of system state equations. In [14], a step-by-step online parameter identification method is proposed, which solves the under-rank problem of multi-parameter identification through the step-by-step identification of resistance, flux linkage, and inductance, ensuring the correctness of identification results and improving the stability of the system.

Taking PMA-SynRM as the control object, a TV-MPCC control strategy based on step parameter identification is proposed in this paper. The method designs six switching combinations and establishes multiple prediction points, considering the current error at each prediction point into the value function. This design results in a more accurate evaluation index and effectively reduces current ripple. To address the susceptibility of TV-MPCC control performance to external disturbances, an MRAS is implemented to sequentially identify the d -axis inductance, q -axis inductance, resistance, and flux linkage parameters of the motor, which improve the robustness of the system.

* Corresponding author: Aide Xu (aidexu@dlmu.edu.cn).

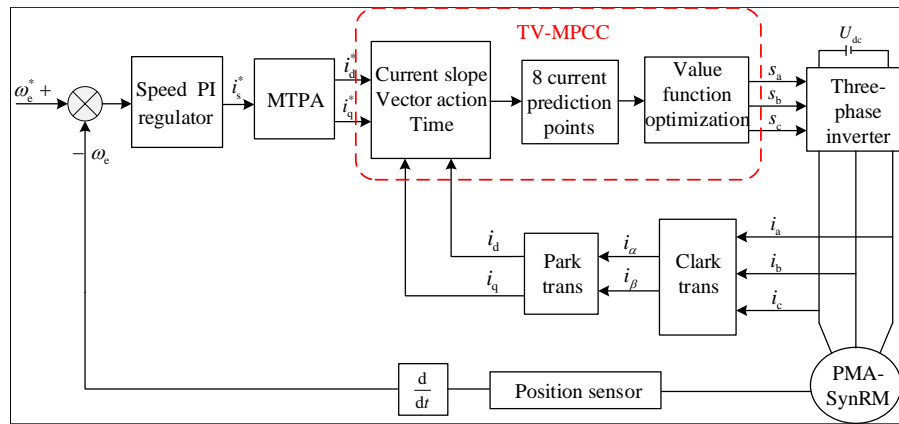


FIGURE 1. Block diagram of TV-MPCC.

2. MPCC STRATEGY ANALYSIS

2.1. Principle of TV-MPCC

Figure 1 shows the block diagram of the control strategy employed under matched parameters conditions. The velocity loop is controlled by proportional integral (PI), and the reference value of its output stator current is passed through MTPA to get the reference current i_d^*, i_q^* . The reconstructed value function is utilized to optimize the current generated under the action of the voltage vector, and the voltage vector corresponding to the smallest value function is selected. Its switching state and the corresponding action time are used to control the on-off of the six switching devices of the three inverter bridges, so as to act on the motor.

The voltage, flux linkage, and torque equations of the d and q axis coordinate system of the motor are formulated as follows:

$$\begin{cases} u_d = Ri_d - \omega_e L_q i_q + \frac{d\psi_d}{dt} \\ u_q = Ri_q + \omega_e L_d i_d + \frac{d\psi_q}{dt} \end{cases} \quad (1)$$

$$\begin{cases} \psi_d = L_d i_d \\ \psi_q = L_q i_q - \psi_f \end{cases} \quad (2)$$

$$T_e = \frac{3}{2} n_p [(L_d - L_q) i_d i_q + \psi_f i_d] \quad (3)$$

where i_d, i_q and u_d, u_q are the d and q axis components of the stator current and voltage vectors; R is the winding phase resistance; ω_e is the rotor angular velocity; L_d, L_q are the inductances of the direct and quadrature axes; ψ_f is the flux linkage; n_p is the number of motor pole pairs.

Equation (1) can be obtained by the forward Euler equation:

$$\begin{cases} i_d(k+1) = \frac{T_s}{L_d} (u_d(k) - Ri_d(k) + \omega_e L_q i_q(k) - \omega_e \psi_f) + i_d(k) \\ i_q(k+1) = \frac{T_s}{L_q} (u_q(k) - Ri_q(k) - \omega_e L_d i_d(k)) + i_q(k) \end{cases} \quad (4)$$

where $i_d(k+1), i_q(k+1)$ are the predicted values of d and q axis currents at the $k+1$ moment; $i_d(k), i_q(k)$ are the d and

q axis currents at the k moment; $u_d(k), u_q(k)$ are the d and q axis voltages at the k moment.

To reduce switching frequency and minimize current ripple, the designed switching sequence is presented in Table 1. $v_{0,7}$ is the zero voltage vector, and v_1 to v_6 are the effective voltage vectors. The numbering of the switching sequences corresponding to the first sector is shown in Fig. 2.

TABLE 1. Sequence of vectors.

Number	Voltage vector sequence
1	$v_0, v_1, v_2, v_7, v_2, v_1, v_0$
2	$v_0, v_3, v_2, v_7, v_2, v_3, v_0$
3	$v_0, v_3, v_4, v_7, v_4, v_3, v_0$
4	$v_0, v_5, v_4, v_7, v_4, v_5, v_0$
5	$v_0, v_5, v_6, v_7, v_6, v_5, v_0$
6	$v_0, v_1, v_6, v_7, v_6, v_1, v_0$

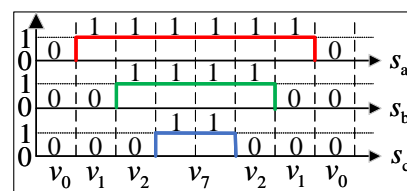


FIGURE 2. Switch sequence of the first sector.

Taking sector 1 in Fig. 2 as the column, the adjacent effective voltage vectors are $v_1(100), v_2(110)$, and the corresponding switching sequence is $v_0(000), v_1(100), v_2(110), v_7(111)$. When switching voltage vectors, only the state of one switching tube changes, reducing the switching loss.

Applying a current gradient transformation to Eq. (1) reveals the effect of each voltage vector on the current:

$$\begin{cases} s_{d0} = \frac{di_d}{dt} |_{u_d=0} = \frac{1}{L_d} (-Ri_d(k) + \omega_e L_q i_q(k) - \omega_e \psi_f) \\ s_{q0} = \frac{di_q}{dt} |_{u_q=0} = \frac{1}{L_q} (-Ri_q(k) - \omega_e L_d i_d(k)) \end{cases} \quad (5)$$

$$\begin{cases} s_{dni} = s_{d0} + \frac{u_{dni}(k)}{L_d} \\ s_{qni} = s_{q0} + \frac{u_{qni}(k)}{L_q} \end{cases} \quad (6)$$

$$\begin{cases} s_{dnj} = s_{d0} + \frac{u_{dnj}(k)}{L_d} \\ s_{qnj} = s_{q0} + \frac{u_{qnj}(k)}{L_q} \end{cases} \quad (7)$$

where s_{d0} , s_{q0} are the slopes of the d and q axis currents when the zero voltage vector is acting; s_{dni} , s_{qni} and s_{dnj} , s_{qnj} are the slopes of the d and q axis currents when the V_{ni} , V_{nj} act in the n th switching sequence; $u_{dni}(k)$, $u_{qni}(k)$ are the components of V_i in the d and q axes in the n th switching sequence; $u_{dnj}(k)$, $u_{qnj}(k)$ are the components of V_j in the d and q axes.

The current trajectory of the inverter under the action of the corresponding voltage vector of the switching sequence is shown in Fig. 3, while the current tracking equation can be obtained as:

$$\begin{cases} i_d(k+1) = i_d(k) + 2(s_{dni}t_{ni} + s_{dnj}t_{nj} + 2s_{d0}t_0) \\ i_q(k+1) = i_q(k) + 2(s_{qni}t_{ni} + s_{qnj}t_{nj} + 2s_{q0}t_0) \end{cases} \quad (8)$$

where t_{ni} , t_{nj} are the effective voltage vectors V_{nj} , V_{ni} action times in the n th switching sequence, and t_0 is the zero voltage vector action time.

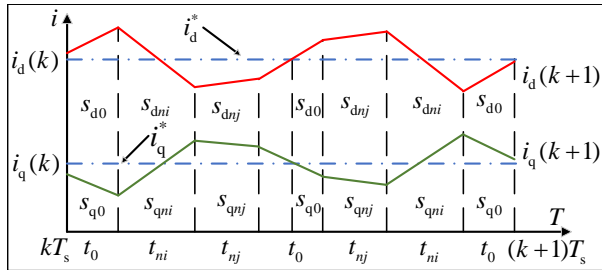


FIGURE 3. Inductance current trace.

The two effective voltage vectors in the sector with zero vector action time can be obtained by associating Eqs. (5) to (8):

$$\begin{cases} t_{ni} = \frac{E_d(s_{qnj} - s_{q0}) + E_q(s_{d0} - s_{dnj})}{2X} + \frac{T_s(s_{q0}s_{dnj} - s_{qnj}s_{d0})}{2X} \\ t_{nj} = \frac{E_d(s_{q0} - s_{qni}) + E_q(s_{dni} - s_{d0})}{2X} + \frac{T_s(s_{qni}s_{d0} - s_{q0}s_{dni})}{2X} \\ t_0 = (T_s/2 - t_{ni} - t_{nj}) \end{cases} \quad (9)$$

where:

$$\begin{cases} E_d = i_d^* - i_d(k) \\ E_q = i_q^* - i_q(k) \\ X = (s_{q0}s_{dnj} + s_{qni}s_{d0} + s_{qnj}s_{dni} - s_{qni}s_{dnj} - s_{qnj}s_{d0} - s_{q0}s_{dni}) \end{cases} \quad (10)$$

As shown in Fig. 3, the d and q axis currents generate multiple prediction points within one control period under the influence of the voltage vector. To more accurately evaluate the predicted current generated by each voltage vector, this paper reconstructs the value function, incorporating the current error at each stage of the voltage vector application. The reconstructed value function can be expressed as follows:

$$G = \sum_{z=1}^8 (i_d^* - i_{d,z})^2 + (i_q^* - i_{q,z})^2 \quad (11)$$

where $i_{d,z}$, $i_{q,z}$ are the current values obtained after the z th segment of voltage vector action in a switching combination. The specific formula is as follows:

$$\begin{cases} i_{d,z+1} = i_{d,z} + s_{dnz}t_{nz} \\ i_{q,z+1} = i_{q,z} + s_{qnz}t_{nz} \end{cases} \quad (12)$$

where t_{nz} is the action time of the z th voltage vector in the n th switching sequence. When the value function is minimized, the obtained switching sequence is the optimal switching sequence, and the corresponding voltage vector action time is the optimal action time.

2.2. Parameter Mismatch Impact Analysis

The stability of the TV-MPCC system is closely related to the accuracy of the d and q axis current slopes. During motor operation, parameters mismatch can arise due to external environmental disturbances and other factors. Taking the inductor parameter mismatch as an example, Eq. (7) is the rate of change of d and q axis currents when motor parameters are accurate, assuming that the inductor parameter mismatch error is ΔL_d , ΔL_q . Under these conditions, d and q axis current slope is as shown in Eq. (13):

$$\begin{cases} \bar{s}_{dnj} = \frac{(u_{dnj}(k) - Ri_d(k) + \omega_e L_q i_q(k) - \omega_e \psi_f)}{L_d + \Delta L_d} \\ \bar{s}_{qnj} = \frac{(u_{qnj}(k) - Ri_q(k) - \omega_e L_d i_d(k))}{L_q + \Delta L_q} \end{cases} \quad (13)$$

From Eq. (7) and Eq. (13), the error in the rate of change of current for the mismatch of d and q axis inductance parameters is:

$$\begin{cases} \bar{s}_{dnj} - s_{dnj} = \frac{\Delta L_d}{L_d + \Delta L_d} \left(\frac{-u_{dnj}(k) + Ri_d(k)}{L_d} + \frac{\omega_e \psi_f - \omega_e L_q i_q(k)}{L_d} \right) \\ \bar{s}_{qnj} - s_{qnj} = \frac{\Delta L_q}{L_q + \Delta L_q} \left(\frac{-u_{qnj}(k) + Ri_q(k)}{L_q} + \frac{\omega_e L_d i_d(k)}{L_q} \right) \end{cases} \quad (14)$$

Equation (14) can be simplified as follows:

$$\begin{cases} \bar{s}_{dnj} - s_{dnj} = -\frac{\Delta L_d}{L_d + \Delta L_d} s_{dnj} \\ \bar{s}_{qnj} - s_{qnj} = -\frac{\Delta L_q}{L_q + \Delta L_q} s_{qnj} \end{cases} \quad (15)$$

According to Eq. (15), mismatched inductance parameters introduce errors in the current slope calculation, resulting in changes in the distribution of voltage vector action times and affecting both control performance and prediction accuracy. Therefore, incorporating an MRAS into the TV-MPCC can effectively enhance system stability in the presence of parameter perturbations.

3. PARAMETRIC ADAPTIVE CONTROLLER DESIGN

In this paper, a step-by-step identification method is adopted, and the inductance parameters of d and q axes are identified first. The actual motor is used as the reference model with

mathematical model as the adjustable model, and the reference model is equation as follows:

$$p i = A i + B u + C \quad (16)$$

where p is a differential operator, $i = [i_d \ i_q]^T$,

$$u = [u_d \ u_q]^T, \quad A = \begin{bmatrix} -R\hat{m} & \omega_e \frac{\hat{m}}{\hat{n}} \\ -\omega_e \frac{\hat{n}}{\hat{m}} & -R\hat{n} \end{bmatrix}, \quad B = \begin{bmatrix} m & 0 \\ 0 & n \end{bmatrix},$$

$$C = \begin{bmatrix} -\omega_e \psi_f \hat{n} \\ 0 \end{bmatrix}, \quad 1/L_d = m, \quad 1/L_q = n. \quad \text{Design the motor adjustable model as follows:}$$

$$p \hat{i} = \hat{A} \hat{i} + \hat{B} u + \hat{C} \quad (17)$$

$$\text{where } \hat{A} = \begin{bmatrix} -R\hat{m} & \omega_e \frac{\hat{m}}{\hat{n}} \\ -\omega_e \frac{\hat{n}}{\hat{m}} & -R\hat{n} \end{bmatrix}, \quad \hat{B} = \begin{bmatrix} \hat{m} & 0 \\ 0 & \hat{n} \end{bmatrix}, \quad \hat{C} =$$

$$\begin{bmatrix} -\omega_e \psi_f \hat{n} \\ 0 \end{bmatrix}, \quad \hat{i} = [\hat{i}_d \ \hat{i}_q]^T, \quad 1/\hat{L}_d = \hat{m} \text{ is the } D\text{-axis in-}$$

ductance discrimination value, and $1/\hat{L}_q = \hat{n}$ is the Q -axis inductance discrimination value. Subtract the reference model from the adjustable model to get:

$$\begin{aligned} p e &= A i + B u + C - (\hat{A} \hat{i} + \hat{B} u + \hat{C}) \\ &= A e + \Delta A \hat{i} + \Delta B u + \Delta C \end{aligned} \quad (18)$$

$\Delta A \hat{i} + \Delta B u + \Delta C = -w$, Eq. (18) can be written as:

$$p e = A e - I w \quad (19)$$

According to the above equations, the PMA-SynRM MRAS can be equated to a nonlinear feedback system, and the structural block diagram is shown in Fig. 4:

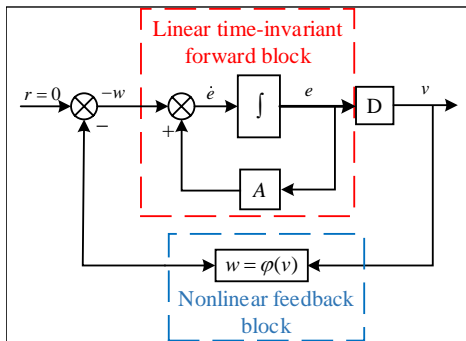


FIGURE 4. The equivalent nonlinear feedback system.

The equation of state for a linear constant forward square is as follows:

$$\begin{cases} \dot{e} = A e + I(-w) \\ v = D e \end{cases} \quad (20)$$

According to Popov's superstability theory, to maintain the stability of the feedback system, it is necessary to demonstrate that the linear system is strictly positively real. This is achieved by finding positive definite matrices P and Q such that Eq. (21) holds, expressed as:

$$\begin{cases} P A + A^T P = -Q \\ P I^T = D \end{cases} \quad (21)$$

Taking P and D as unit matrices and assuming that A is a negative definite matrix, there must exist a positive definite matrix Q such that the linear definite forward square is strictly positively real. Additionally, it is necessary to ensure that the nonlinear feedback loop satisfies the Popov integral inequality:

$$\eta(t_0, t_1) = \int_{t_0}^{t_1} w^T v dt \geq -\gamma_0^2 \quad (22)$$

Substituting the values of v , w into the Popov integral inequality of the above equation can derive the adaptive law for the d and q axis inductances as follows:

$$\begin{cases} \frac{1}{\hat{L}_d} = \frac{1}{L_d} + (k_{p1} + \frac{k_{i1}}{s}) (i_d - \hat{i}_d) (u_d - \omega_e \psi_f) \\ \frac{1}{\hat{L}_q} = \frac{1}{L_q} + (k_{p2} + \frac{k_{i2}}{s}) (i_q - \hat{i}_q) u_q \end{cases} \quad (23)$$

After identifying d and q axis inductance parameters, the second-level MRAS is applied to identify the flux linkage and resistance parameters. The adaptive law for resistance, flux linkage identification follows a similar design process of d and q axis inductances, and the adaptive rate of resistance and magnetic chain can be determined by substituting w_1 , v_1 into Popov's integral inequality:

$$\begin{cases} \hat{R} = R + (k_{p1} + \frac{k_{i1}}{s}) \left(-\frac{1}{L_d} \hat{i}_d (i_d - \hat{i}_d) - \frac{1}{L_q} \hat{i}_q (i_q - \hat{i}_q) \right) \\ \hat{\psi}_f = \psi_f + (k_{p2} + \frac{k_{i2}}{s}) \left(-\omega_e \frac{1}{L_d} (i_d - \hat{i}_d) \right) \end{cases} \quad (24)$$

Incorporating the adaptive rates for online identification of d and q axis inductances, the block diagram of step-by-step parameter identification process is illustrated in Fig. 5.

The above parameter identification strategy is integrated into TV-MPCC, and the four motor parameters in the controller are corrected in real time using the identified values. This ensures that the parameters in the motors and controller are kept matched, so that the control effect of TV-MPCC can be optimized, and the control block diagram is shown in Fig. 6.

4. SIMULATION RESULTS ANALYSIS

To verify the accuracy and effectiveness of the proposed algorithm, simulations are performed in Matlab/Simulink. The motor parameters of the used PMA-SynRM are shown in Table 2. The switching frequency is 10 kHz, and the sampling time is 100 μ s.

4.1. Simulation Validation of Parameter Identification Algorithm

The stability of the identified values of the algorithm proposed in this paper for d and q axis inductances, resistances, and flux linkages is first verified. In order to make the identification equation full rank step-by-step identification is used. The simulation conditions are set to the reference speed of 1000 r/min, and load torque is 5 N · m.

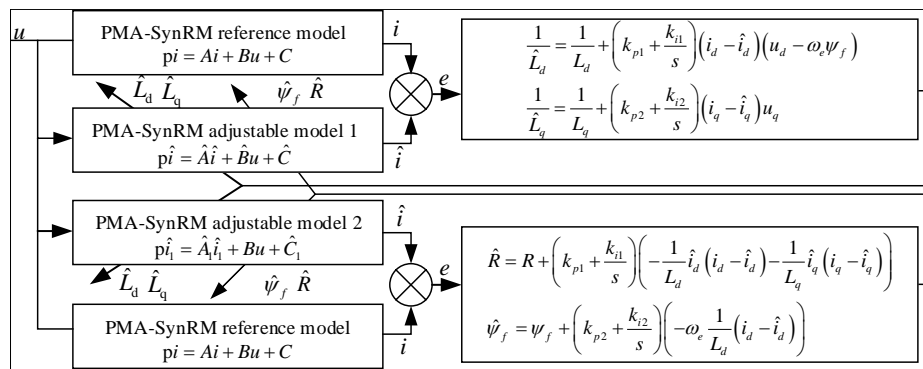


FIGURE 5. Structure block diagram of four-parameter step identification based on MRAS.

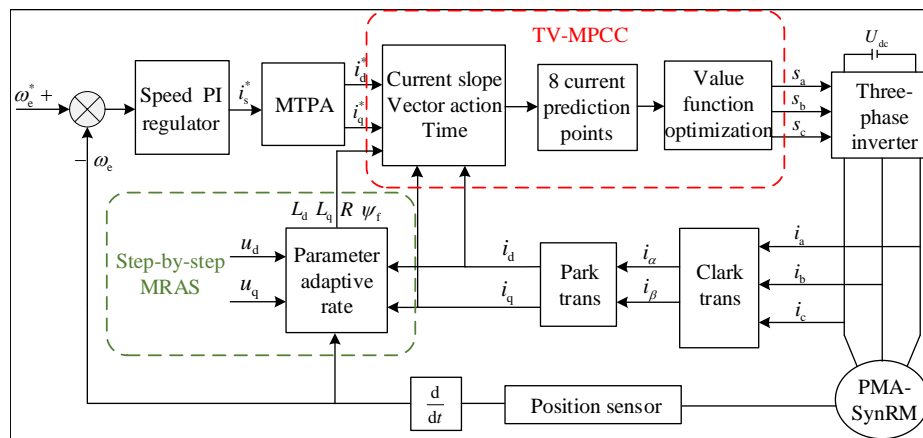


FIGURE 6. Block diagram of TV-MPCC algorithm based on step-by-step parameter identification.

TABLE 2. Parameters of PMA-SynRM.

Parameter/Unit	Value
Pole pairs	3
Rated power/kW	3
Rated torque/N · m	9.5
Rated speed/r/min	30000
Rated voltage/V	380
Rotor resistance/Ω	2.8
Flux/Wb	0.19
Ld/mH	19.7
Lq/mH	5.3

The simulation results in Fig. 7 demonstrate that the identified values of d and q axis inductances, resistances, and flux linkages stabilize near the reference values, and the convergence error is less than 3%, which has a high identification accuracy.

4.2. TV-MPCC Steady State Simulation

Secondly, the steady state performance of TV-MPCC is verified under matched motor parameters. The simulation is conducted with a reference speed of 1000 r/min and the load torque

of 5 N · m. i_d^* , i_q^* and i_d , i_q represent the predicted current and sampling current of the d and q axes, respectively.

As shown in Fig. 8, the fluctuation of the actual d -axis current is maintained at 0.024 A and the fluctuation of the actual q -axis current maintained at 0.083 A during the steady state operation of the TV-MPCC under the parameter matching condition. This indicates that the TV-MPCC has a good tracking accuracy and steady state effect, and the control performance is good.

4.3. Steady State Simulation Verification of the Proposed Algorithm

To simulate motor parameter mismatch, this paper adjusts the initial value of the parameter model. First, a mismatch of d -axis inductance is simulated by setting the motor d -axis inductance to more than twice of the actual motor parameters at the beginning of simulation, and MRAS is introduced at 0.2 s to identify and correct the d -axis inductance parameter of the system online. The PMA-SynRM reference speed is set to 1000 r/min, and the load torque is 5 N · m to verify the algorithm proposed in this paper. d and q axis current waveforms and reference current waveforms are shown in Fig. 9.

As shown in Fig. 9, when the d -axis inductance parameter is mismatched, the d and q axis currents exhibit ripples and increase the peak values of the d and q axis currents which negatively impacts current stability and tracking accuracy. Sec-

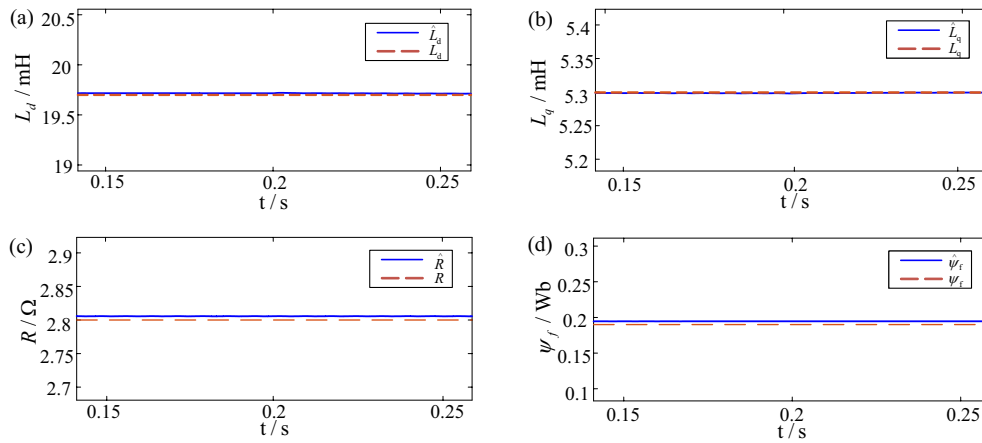


FIGURE 7. Four parameter step identification simulation diagram. (a) d axis inductance, (b) q axis inductance, (c) stator resistance, (d) flux linkage.

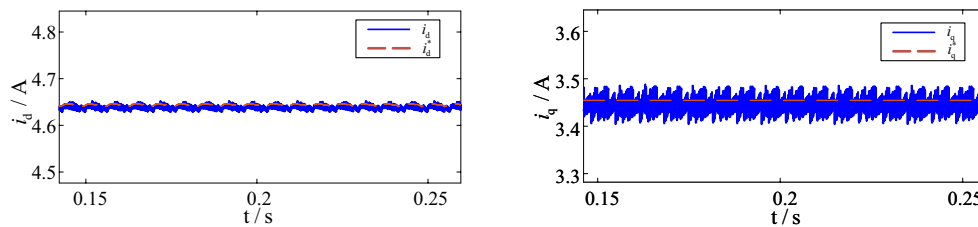


FIGURE 8. Current waveform diagram of TV-MPCC with parameters match.

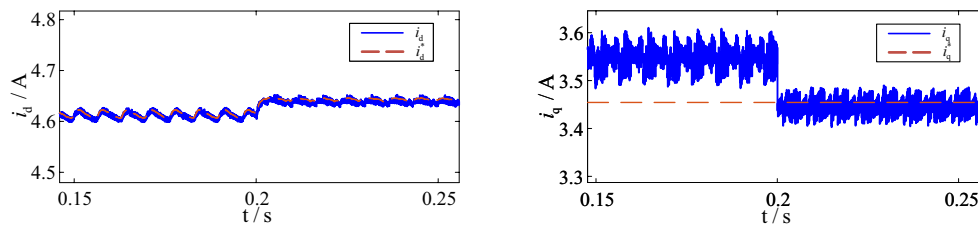


FIGURE 9. Simulation waveform diagram of proposed algorithm with d -axis inductance parameter mismatches.

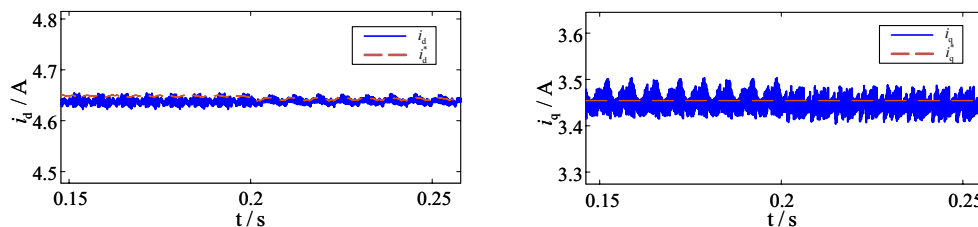


FIGURE 10. Simulation waveform diagram of proposed algorithm with q -axis inductance parameter mismatches.

only, the q -axis inductance parameter mismatch is simulated by setting q -axis inductance to more than twice of the actual motor parameters, and other simulation conditions remain unchanged, the proposed algorithm is verified, and the waveforms are shown in Fig. 10.

When the q -axis inductance parameter is mismatched, the system's stability is compromised. The tracking effect of d -axis current becomes worse, and the peak value of q -axis current fluctuation also increases, which further proves the instability of the control system when the parameters are mismatched.

With the same simulation conditions, the stator resistance is set to more than twice of the actual motor parameters to simulate the proposed algorithm's performance under resistance parameters mismatch. The waveform diagram is shown as follows.

Figure 11 illustrates that stator resistance parameter mismatch degrades d and q axis currents tracking accuracy, resulting in positive errors. Finally, the proposed algorithm for the mismatch of flux linkage parameter is verified by simulation.

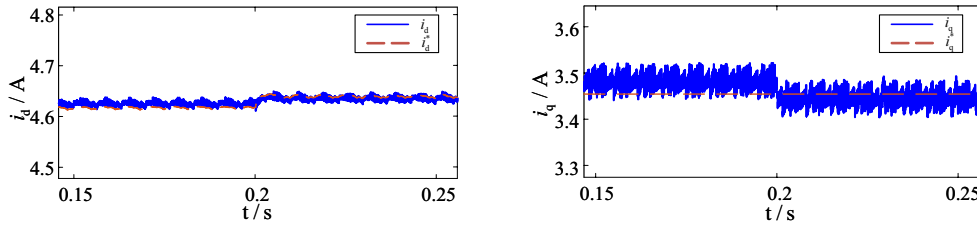


FIGURE 11. Simulation waveform diagram of proposed algorithm with stator resistance parameter mismatches.

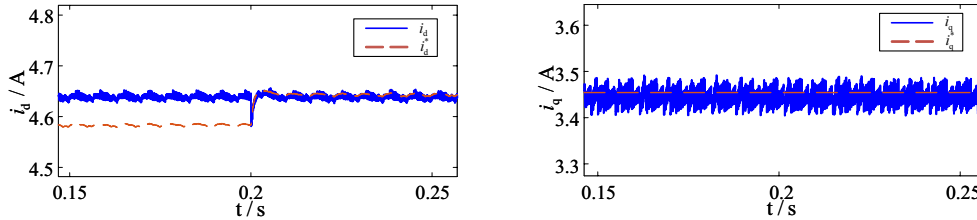


FIGURE 12. Simulation waveform diagram of proposed algorithm with flux linkage parameter mismatches.

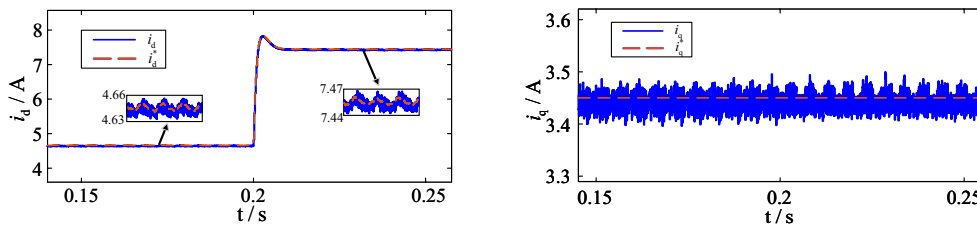


FIGURE 13. Dynamic simulation waveform of the proposed algorithm when the parameters mismatch.

TABLE 3. Current result comparison.

Motor parameter	Current fluctuation/A		Current error/mA	
	$\Delta i_d/A$	$\Delta i_q/A$	e_{id}/mA	e_{iq}/mA
L_d parameter mismatch	0.031	0.129	-9	98
L_q parameter mismatch	0.039	0.089	-11	-15
R parameter mismatch	0.028	0.086	11	37
ψ_f parameter mismatch	0.029	0.554	71	-10
Proposed algorithm	0.026	0.085	-4	-9

Figure 12 demonstrates that flux linkage parameter mismatch degrades TV-MPCC performance, notably causing significant tracking errors in the d -axis current.

As shown in the simulation diagrams, after MRAS is introduced at 0.2s to accurately identify the motor parameters and correct the motor parameters in TV-MPCC controller, the peak values of the d and q axis current fluctuations are significantly reduced; the oscillation phenomenon disappears; and the current tracking accuracy is the same as the parameter matching.

In order to clearly illustrate the improvement of the proposed algorithm, Table 3 provides the data of current fluctuation and current tracking error of d - q axis when parameters mismatch between traditional TV-MPCC and the proposed algorithm occurs. The expression of current tracking error is defined as fol-

lows:

$$\begin{cases} e_{id} = i_d(k+1) - i_d^* \\ e_{iq} = i_q(k+1) - i_q^* \end{cases} \quad (25)$$

4.4. Dynamic State Simulation Verification of the Proposed Algorithm

In order to further verify the effectiveness of the proposed algorithm, the speed is set at 1300 r/min, and the load torque jumps from $5 \text{ N} \cdot \text{m}$ to $8 \text{ N} \cdot \text{m}$ at 0.2 s.

As shown in Fig. 13, in the case of parameters mismatch, the proposed algorithm still has good control effect after 0.2 s torque jump; the peak value of d -axis current is 0.027 A; the peak value of q -axis current is 0.086 A, which has good dynamic performance.

5. CONCLUSION

To address the sensitivity of the TV-MPCC algorithm for PMA-SynRM to external disturbances, a TV-MPCC algorithm based on step-by-step parameter identification is proposed in this paper. Simulation results demonstrate that the TV-MPCC algorithm has good current tracking accuracy and control performance. However, the mismatch of parameters adversely affects stability, increases current fluctuations, and degrades tracking characteristics. By introducing an MRAS to identify and correct d and q -axis inductances, resistances, and fluxes of the motor in real time, the adverse effects of parameter mismatch are effectively mitigated, reducing the peak values of d and q -axis currents, enhancing tracking characteristics, and improving system stability.

REFERENCES

- [1] Jia, S., P. Zhang, D. Liang, M. Dai, and J. Liu, "Design and comparison of three different types of efficiency machines," in *2019 22nd International Conference on Electrical Machines and Systems (ICEMS)*, 1–4, Harbin, China, 2019.
- [2] Cao, H., M. Ai, and Y. Wang, "Research status and development trend of permanent magnet assisted synchronous reluctance motor," *Transactions of China Electrotechnical Society*, Vol. 37, No. 18, 4575–4592, 2022.
- [3] Zheng, S. Y., X. Y. Zhu, L. Xu, *et al.*, "Design and performance analysis of PM-assisted synchronous reluctance motor considering high torque-quality ratio," *Chinese Journal of Electrical Engineering*, Vol. 42, No. 19, 7236–7248, 2022.
- [4] Leuzzi, R., P. Cagnetta, S. Ferrari, P. Pescetto, G. Pellegrino, and F. Cupertino, "Transient overload characteristics of PM-assisted synchronous reluctance machines, including sensorless control feasibility," *IEEE Transactions on Industry Applications*, Vol. 55, No. 3, 2637–2648, 2019.
- [5] Huang, H. and Y. S. Hu, *Design and Application of Permanent Magnet Assisted Synchronous Reluctance Motor*, Machinery Industry Press, 2017.
- [6] Chen, Y., B. Baodong, C. Dezhi, *et al.*, "Design and analysis of a variable flux permanent magnet assisted synchronous motor," *Transactions of China Electrotechnical Society*, Vol. 34, No. 3, 489–496, 2019.
- [7] Niazi, P., H. A. Toliyat, and A. Goodarzi, "Robust maximum torque per ampere (MTPA) control of PM-assisted SynRM for traction applications," *IEEE Transactions on Vehicular Technology*, Vol. 56, No. 4, 1538–1545, 2007.
- [8] Davari, S. A., D. A. Khaburi, and R. Kennel, "An improved FCS-MPC algorithm for an induction motor with an imposed optimized weighting factor," *IEEE Transactions on Power Electronics*, Vol. 27, No. 3, 1540–1551, 2012.
- [9] Xu, Y., B. Zhang, and Q. Zhou, "Two-vector based model predictive current control for permanent magnet synchronous motor," *Transactions of China Electrotechnical Society*, Vol. 32, No. 20, 222–230, 2017.
- [10] Wang, C., "Research on current control strategy of permanent magnet synchronous motor with double vector model prediction," Ph.D. dissertation, Harbin University of Science and Technology, Harbin, China, 2022.
- [11] Xu, Y., J. Wang, B. Zhang, and Q. Zhou, "Three-vector-based model predictive current control for permanent magnet synchronous motor," *Transactions of China Electrotechnical Society*, Vol. 33, No. 5, 980–988, 2018.
- [12] Li, X. and R. Kennel, "General formulation of Kalman-filter-based online parameter identification methods for VSI-fed PMSM," *IEEE Transactions on Industrial Electronics*, Vol. 68, No. 4, 2856–2864, 2021.
- [13] Gao, F. Y., D. H. Luo, M. M. Li, *et al.*, "Predictive current control of permanent magnet synchronous motor with on-line correction of mismatch parameters," *Control Theory & Applications*, Vol. 38, No. 05, 603–614, 2021.
- [14] Li, Y. J., X. Dong, H. F. Wei, *et al.*, "Parameter identification of permanent magnet synchronous motor based on improved model reference adaptive system," *Control Theory & Applications*, Vol. 37, No. 09, 1983–1988, 2019.